International Journal of Advanced Engineering and Management Research

Vol. 11, No. 01; 2026

ISSN: 2456-3676

A Control System for Smart Drone

Nickolay Zosimovych[1]
[1]State University "Kyiv Aviation Institute", Aerospace Faculty,
Kyiv, Liubomyra Guzara Ave., 1, KAI, 03058, Ukraine

doi.org/10.51505/ijaemr.2026.1103 URL: http://dx.doi.org/10.51505/ijaemr.2026.1103

Received: Dec 06, 2025 Accepted: Dec 22, 2025 Online Published: Feb 02, 2026

Abstract
This paper presents a hierarchical flight control system for smart tilt-rotor drones. The proposed methodology performs high-level mission goals by gradually verifying them into machine-level commands. The learned data from various sensors is spread backside to the greater levels for sensitive decision making. Each vertical take-off and landing drone is linked through standard wireless communication rules for an accessible multi-agent facility. The proposed flight control system has been effectively used on various types of smart tilt-rotor drones and has been validated in specific applications. Results from waypoint navigation, a probabilistic chase-evasion competition, and vision-based object chasing show the capability of the recommended method for intelligent drones.

Keywords: Tilt-rotor drone (TRD), vertical take-off and landing (VTOL), control, vehicle control language (VCL), inertial navigation system (INS), and global positioning system (GPS)

1. Introduction

Implementation of smart drones has been done potential because of hi-tech innovations in different areas such as artificial intelligence, flying robotics, wireless communication, and control systems.

Tilt-Rotor vertical take-off and landing (VTOL) or tilt-rotor drones (TRDs) have distinctive flying abilities such as hover, vertical take-off/landing, and sideslip, which cannot be attained by traditional fixed-wing airplanes (CH-10, 2021, Sheng, 2018). These multipurpose mission modes are effective for numerous circumstances as well as reconnaissance, ground target tracking, and tasks with restricted launching space such as a ship deck or in situations that need repeated landings and take-offs (Fig. 1) (Vertical-landing, 2023, Zosimovych, 2024). These types of drones integrated are helicopter technology as fixed-wing aircraft technology.

However, the recent level still drops quickly by applying the results to most actual applications and using the detailed abilities of the rotorcraft. Our research has focused on enhancing the performance of TRDs as participants of a networked intelligent group containing numerous heterogeneous drones. To reach this goal, it is important that every mission control system be able with well-capable autonomy, i.e., abilities to independent sense, mind, plan, and act in

Vol. 11, No. 01; 2026

ISSN: 2456-3676

expertise with other drones or ground/ water-based robots or environments. This article shows the combination of a hierarchical flight management system (FMS) for smart TRDs that offers autonomy as permitting management among all team participants.

The general control structure contains two cascade PID controllers, which accept errors from speed and attitude and provide consistent control amounts (Wang, 2024). The control of TRD is achieved by applying the negative feedback (Zosimovych, 2020).

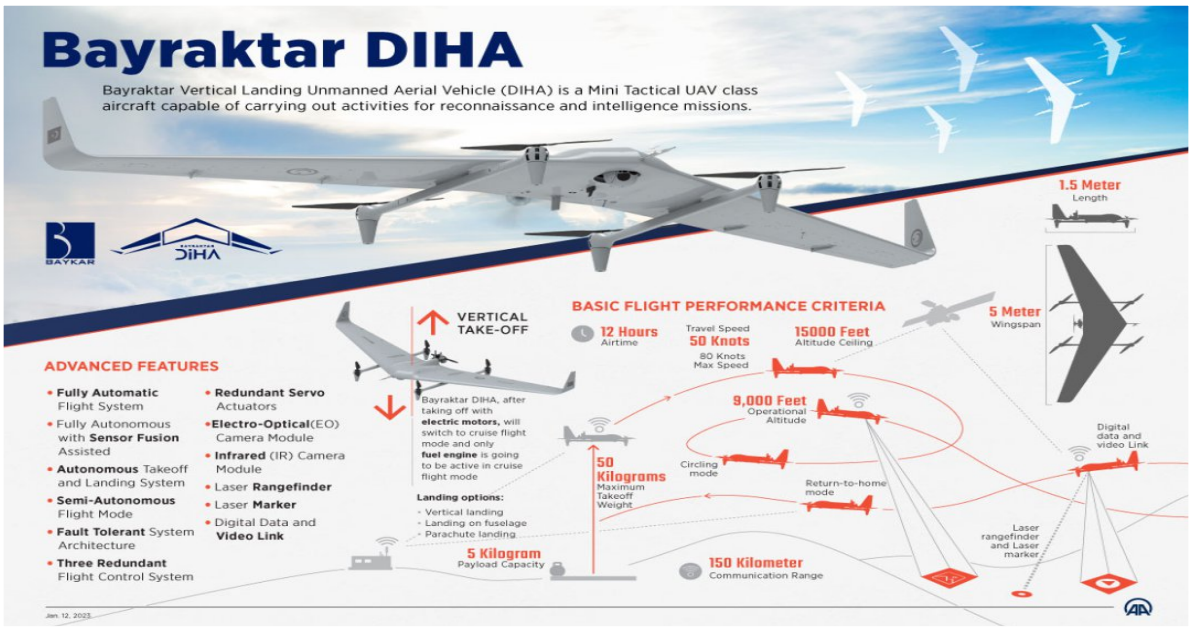

Figure 1. Bayraktar DİHA vertical landing unmanned aerial vehicle

Additionally, the current drone controller offers the off-the-shelf controller for this type of drone, it normally needs to load up the appropriate files to represent the required control pull to every single actuator input, which can only carry the drone with a fixed structure. In its place, we employed a possible drone structure change (such as an actuator failure).

Vol. 11, No. 01; 2026

ISSN: 2456-3676

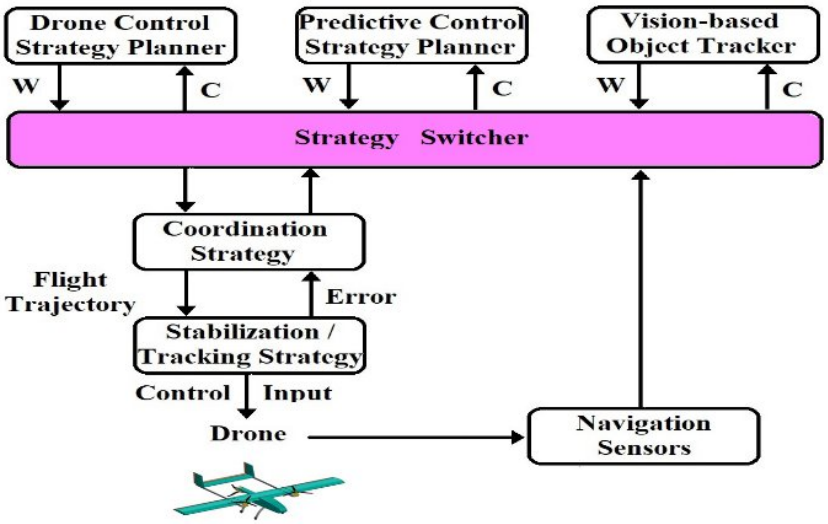

Figure 2. Hierarchical FMS for smart TRD: W – waypoints, C–conflicts

Therefore, we use a multi-differential controller as a non-linear model predictive tracking controller (Fig. 2) (Zosimovych, 2024).

As target problems, these situations are considered: waypoint navigation, pursuit-evasion, ground target tracking, and vision-based landing (Kim, 2023). These strategies represent one or more functionalities of the hierarchical multi-agent system. In the waypoint navigation, the functionality of the guidance strategy using the VCL structure is underlined. Pursuit-evasion refers to the probabilistic logic for the strategy switcher, multiagent synchronization on a wireless network, dynamic VCL process, and vision-based detection.

2. Problem Statement

An intelligent agent functions as follows: 1) constantly identifies dynamically varying environments; 2) to explain apparent data, to resolve tasks and to define suitable reactions; and 3) shows suitably to impact terms in its environment (Kim, 2023). Based on these properties, we could depict each strategy in the hierarchical FMS shown in Fig. 2 (Zosimovych, 2024).

Figure 2 reveals three types of strategy planners to be applied for every test. The suitable strategy planner for a particular mission is chosen by a strategy switcher (Zosimovych, 2024).

While the recent status of the world is not totally significant, the world is modeled as a partly detectable Markov decision method. The strategy planner also renews every agent's information, or probability distribution throughout the state space of the world, provides measurement and activity stories, and creates a plan, like a mapping from the agent's principle state to its act set (Kim, 2023). The pursuit of the optimal strategy is computationally problematic in many challenges; therefore, optimal strategies are normally applied in (Kim, 2023), or the group of

Vol. 11, No. 01; 2026

ISSN: 2456-3676

rules to seek over is restricted as in (Zosimovych, 2023). Processes are usually operated on real-time functioning structures to fulfil fast real-time restrictions.

The strategy planner also operates communication networks. Developed from an easy telemetry for data up and down link, communication performs a crucial function in the real-time management of numerous drones in a dynamic environment as a closely coordinated, distributed interacted intelligence. Furthermore, it is necessary to obtain a high-ranking quality-of-service wireless communication system with negligible expectancy, in the spirit of ambient noise or signal blocking for secure action.

Ultimately, the drone is ordered to go to the planned spots that are processed using the decision-making procedure. In acting so, the smart UAS ought to be capable of independently driving itself beyond the reference routes or waypoints. Each drone platform is supplied with alleviating controllers. Special action-detection management appears at an extremely rapid level in charge of surviving possibilities, such as revealing and prevention of collisions (Zosimovych, 2023, Zosimovych, 2024).

2.1 Drone On-board Platform

Modern smart UAS is firmly integrated by mechanical and electronic modules, involving an airframe, navigation sensors, processors, batteries, and extra on-board sensors, targeted at implementing autonomous responsibilities through nominal interference by a remote human operative. Bayraktar DİHA TRD is made on off-the-shelf remote-controlled drones of numerous ranges and loads (Vertical, 2023, Kim, 2003, Zosimovych, 2023, Zosimovych, 2024).

The on-board flight computer is fundamental to the guidance, navigation, and control of the host drone. It is concerned with real-time UAS control, sensor integration, and inter-agent communication. The flight management software system is executed in the real-time operating system. The input to the servo control system is processed at 50 Hz using the flight control algorithms (Kim, 2003, Zosimovych, 2024).

The navigation system is made over INS and GPS. INS delivers position, velocity, attitude angles and levels at an arbitrarily high rate. A weakness of INS is the boundless fault that develops quickly over time. This can be successfully adjusted by an outward locate sensor such as a GPS. Due to the matching features of INS and GPS, a grouping of these sensors has enhanced the universal arrangement for modern UAS.

Bayraktar DİHA TRDs are furnished with an on-board vision handling unit (VHU) and a camera boarded on a tilt platform. The VHU path indicators of the specific model and approximate the virtual flow among the camera and the object. For independent take-off and landing, a vision-created sensing algorithm estimates the comparative space and slope angles to the indicator on the landing site. The VHU approximate is adapted with navigation data starting the onboard computer through a sequential tie (Zosimovych, 2023).

Vol. 11, No. 01; 2026

ISSN: 2456-3676

Wireless networks are employed to realize the remote availability and connectivity amongst numerous agents. The communication stream on the communication connection is labelled in a regulated communication arrangement, which allows the interoperability of airborne and ground-created agents (Kim, 2003, Zosimovych, 2024).

2.2 Drone Dynamics

A TRD is a kindly nonlinear multi-input multi-output (MIMO) system, which is revealed to have a critical disorder such as its peculiar rotor wake and wind gusts. The modelling of the smart UAS merits a dedicated exposure and the complete details of the active simulations, beginning which the suggested control rules are constructed, is observed in (Zosimovych, 2023).

The total dynamics of a TRD are modeled as a set of nonlinear differential equations, which is split into the kinematics (1st two equations) and the system dynamics (the last one) (Kim, 2003, Zosimovych, 2024):

$$\left[\cdot \quad \cdot \quad \cdot\right] \quad \left[\dot{s}^S,\dot{y}^S,\dot{z}^S\right]^T \doteq R^B \to^S \left[\dot{x}^B,\dot{y}^B,\dot{z}^B\right]^T, \tag{1}$$

$$-\left[\ \right] \quad \left[\qquad \right]\begin{bmatrix}\frac{d}{dt}\end{bmatrix}\begin{bmatrix}\phi\\ \Theta\\ \psi\end{bmatrix} = \begin{bmatrix}1 & sin\phi\tan\Theta & cos\phi\tan\Theta\\ 0 & cos\phi & -sin\phi\\ 0 & sin\phi\cos\Theta & cos\phi\cos\Theta\end{bmatrix}, \tag{2}$$

$$\cdot \ (\,) \quad \dot{s}^D(t) = f_c\left(x^D(t),u(t)\right), \tag{3}$$

where:

$$x = \left[x^K,x^D\right]^T \in R^{n_x},$$

$$x^K = \left[x^S,y^S,z^S,\phi,\Theta,\psi\right]^T$$

$$x^D = \left[u,v,w,p,q,r,a_{1s},b_{1s},r_{fb}\right]^T,$$

$$u = \left[u_{a1s},u_{b1s},u_{\Theta M},u_{r_{ref}}\right]^T \in R^{n_x}.$$

At this point, S and B indicate 3-D and body coordinates. $\cdot\ \ddot{x}^B,\dot{y}^B$, and $\cdot\dot{z}^B$ u,v and w correspondingly, will be treated for notational ease) designate velocity regarding the body-coordinated framework. ϕ, Θ, and ψ mean roll, pitch, and yaw, and p,q and r are their rates, respectively (Zosimovych, 2023).

The factors a_{1s} and b_{1s} are longitudinal and lateral flap angles, and r_{fb} is the feedback gyro system state (Pessoa, 2017). The dynamic model, as in Eq. (3), has four enters. u_{a1s} and u_{b1s}

Vol. 11, No. 01; 2026

ISSN: 2456-3676

control lateral and longitudinal repeated pitch, correspondingly. The cyclic pitch changes the original pitch of every rotor blade throughout a cycle to vary the trend of the thrust vector. $u_{\Theta M}$ is the servo system response for the main rotor cooperative pitch. Cooperative control changes the pitch of all blades and thus variations the magnitude of the thrust direction. $u_{r_{ref}}$ controls the amount and direction of the rear rotor thrust, which counters the anti-torque of the front rotor and thus controls the heading angle. Anticipated to the intricacy and ambiguity essential to aerodynamic orders, the dynamic simulation was recognized by using a parametric recognition procedure to a set of test flight statistics. The test data were put on the frequency-curving signals to the instrumented TRD in the longitudinal, lateral, pitch and yaw paths in turn, whilst providing the drone's general stability. The UAV reaction is determined by navigation sensors and transferred to the base station through a wireless link. The verified extent is prepared and then treated by the forecast error technique, a time-domain parametric identification approach (Kay ton, 2006). The following model for the last equation (Eq. (3) is a lined time-invariant structure with the conditions and responses described below.

3. Drone Stabilization and Tracking

In the primary approximate, multiple single-input, single-output (SISO) control loops are aimed across the four inputs of longitudinal / lateral cyclical pitches and main / tail cooperative pitches (Kim, 2003). This consideration has evident benefits in conditions of an easier configuration, basic design practice, and low processing capacity. On the other hand, it does not present a methodical approach to describe improbability, disturbance, and dispersion. Furthermore, it has extremely restricted implies to alleviate the coupling among passages.

The suggested controller contains three loops (Virtual, 2021, Zosimovych, 2024): 1) deepest attitude controller, 2) mid-loop linear velocity controller, and 3) the outer loop attitude controller (Fig. 3).

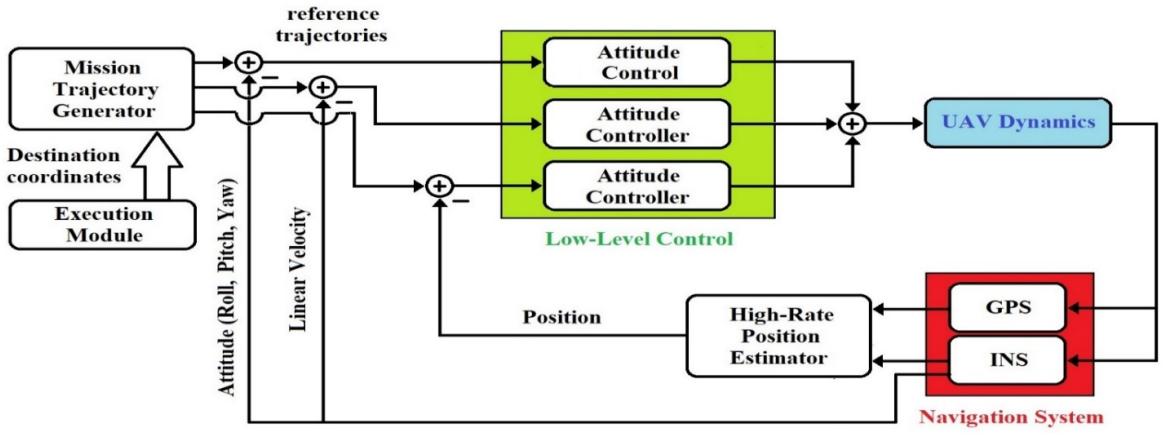

Figure 3. Controller architecture

Vol. 11, No. 01; 2026

ISSN: 2456-3676

The attitude controller supplies reverse only the difference of the roll and pitch angles from the reduced situation (nonzero angle wanted to conserve stability), not the noisy angular rates p and q measured by rate gyros. This methodology produces a controller that is easier and more resistant to mechanical vibration. The suitable angular feedback gains for the roll and pitch channels are established to take appropriate reaction speed and damping ratio (Kim, 2003, Zosimovych, 2024).

For hover control, the position control circles in all 3 (x-, y-, and z) axes are included on the importance of the linear velocity and attitude response. The position control includes domestic coordinate conversion to reward the heading adjustment. The position gains are located by using the related techniques explained over the extended TRD dynamics using velocity and attitude response. Lastly, whole acts are combined to remove steady-state faults and reduce disparity (Kim, 2003).

The vertical and heading dynamics are naturally steady exactly to the interface between the inflow and the induced lift. The vertical reaction is advanced by synthetic dampening via the destructive velocity reaction. For yaw tracing, the route fault and its integral are consumed back on top of the integral gyro system (Zosimovych, 2024).

In brief, the multi-loop PID control law is assumed as the subsequent regular equation (Kim, 2003):

$$\begin{pmatrix} & & \int & \\ & & \int & \\ & \int & & \\ \int & & & \end{pmatrix} \begin{pmatrix} u_{a1s} = -K_{\phi}\phi - K_{\vartheta}\vartheta - K_{y}e_{y}s - K_{Iy}\int e_{y}sdt, \\ u_{b1s} = -K_{\Theta}\Theta - K_{u}u - K_{x}e_{x}s - K_{Ix}\int e_{x}sdt, \\ u_{\Theta M} = -K_{w}w - K_{z}e_{z}s - K_{Iz}\int e_{z}sdt, \\ u_{r_{ref}} = -K_{\Psi}\Psi - K_{I\Psi}\int e_{\Psi}dt, \end{pmatrix} \quad (4)$$

where $e_{x}s$,$e_{y}s$, and $e_{z}s$ indicate the position error, and e_{Ψ} indicates the leading error.

Vol. 11, No. 01; 2026

ISSN: 2456-3676

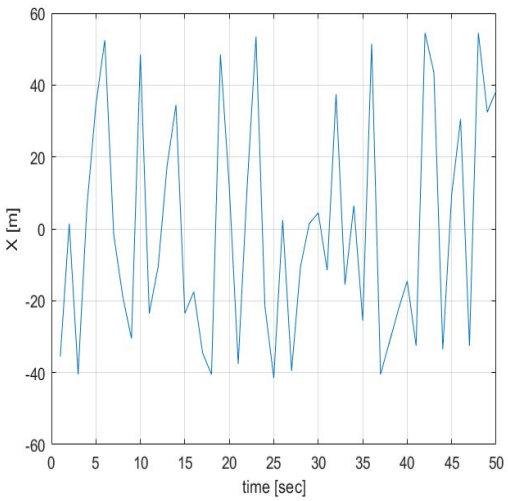

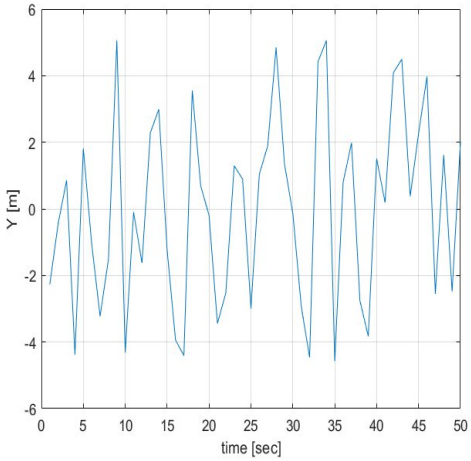

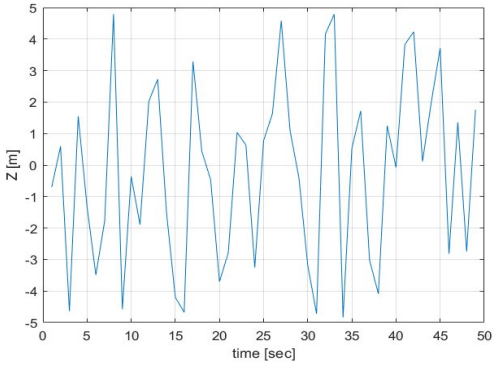

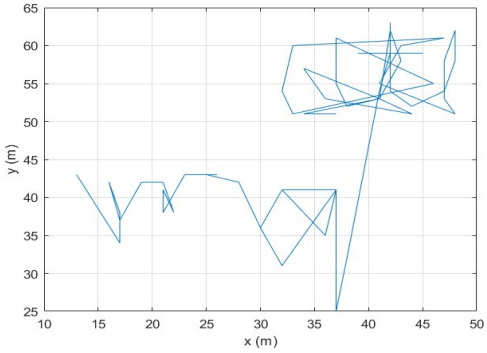

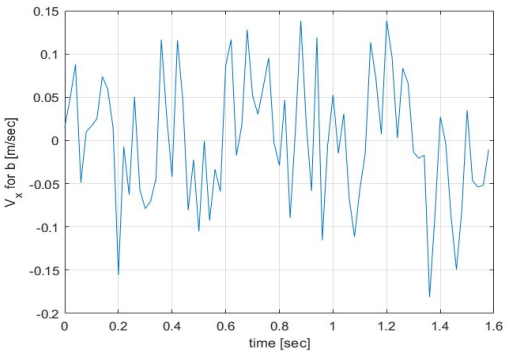

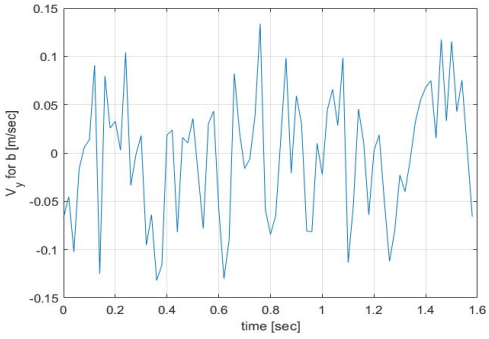

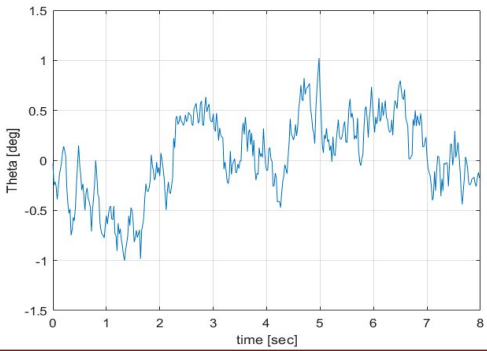

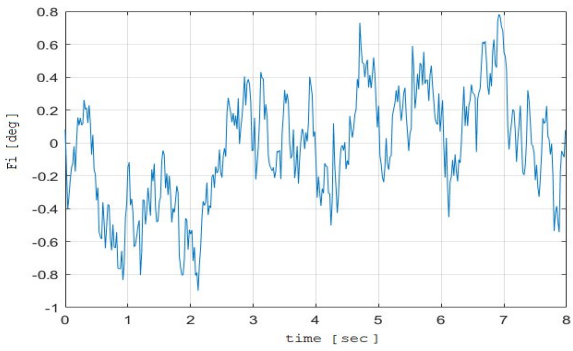

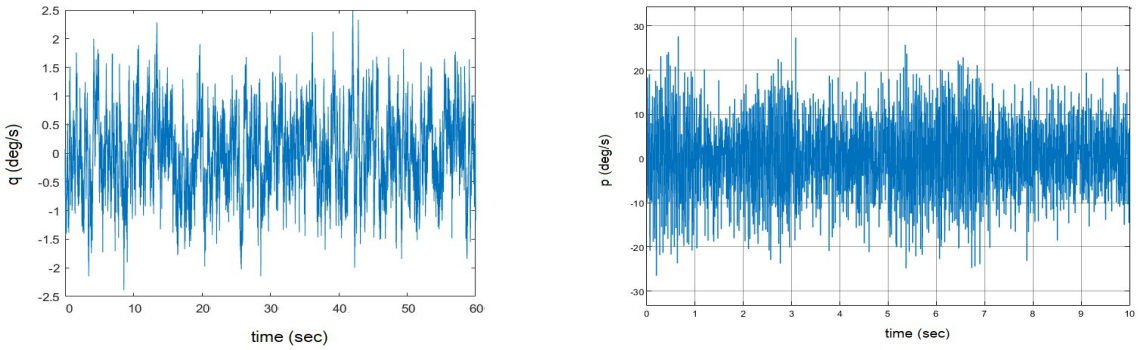

Figure 4. Some experimental results of autonomous hovering

Figure 4 shows the experimental result of the hovering controller tested on the Tilt-Rotor Bayraktar DİHA Unmanned Aerial Vehicle (Turkey) (Vertical, 2023). The RUAV proved a steady and precise control reply through (±0.2; ±0.3; ±0.2 m; $\pm 1.1^0$) correctness in (x; y; z; ψ)-axis. Roll, pitch, and translational velocity in the x and y paths are controlled very well and completely (Zosimovych, 2024).

4. Nonlinear Predictive Controller

Earlier, we have shown that conventional multi-loop control makes a rational fit. To advance the following presentation for composite routes by considering the nonlinear features, link between modes, and input/state capacity, we similarly reflect a nonlinear model prognostic controller as a chasing deposit.

For each model time, a nonlinear predictive controller calculates a determinate control arrangement, which reduces cost function, naturally a weighted quadratic sum of positions and inputs completed a finite distance. We used a discretized core model obtained from a partly nonlinear continuous time model (with nonlinear force footings and complete nonlinear kinematic equations) (Kim, 2003).

As in (Kim, 2003) for the inner model, Eq. (2) is discretized to

$$x_{k+1} = f(x_k, u_k) \triangleq f_d(x_k) + B_d u_k,$$

$$f_d(x_k) \triangleq x_k + T_s f_c(x_k),$$

$$B_d \triangleq T_s B_c, \qquad (5)$$

where T_s is the sample time. For chasing, we describe a cost function as in (Kim, 2003):

$$\left(\tilde{\ }\right) \quad \sum J = \phi\left(\tilde{y}_N\right)\tilde{} + \sum_{k=0}^{N-1} L\left(x_k, \tilde{y}_k, u_k\right) \qquad (6)$$

$$\tilde{\phi}(\tilde{y}_N) \triangleq \frac{1}{2}\tilde{y}_N^T P_0 \tilde{y}_N, \quad (7)$$

$$\tilde{L}(x_k, \tilde{y}_k, u_k) \triangleq \frac{1}{2}\tilde{y}_K^T Q \tilde{y}_k + \frac{1}{2}x_k^T S x_k + \frac{1}{2}u_k^T R u \quad , \quad (8)$$

where $\tilde{y} \triangleq y_d - y, y = Cx + R^{n_y}$, y_d is the desired trajectory, and S is offered to confident the state variables that do not conventional seem in y. By offering an order of Lagrange multiplier vectors $\{\lambda_k \in R^{n_x}\}_{k=1}^{N}$, as in (Kim, 2003):

$$J = \tilde{\phi}(\tilde{y}_N) + \sum_{k=0}^{N-1}[L(x_k, \tilde{y}_k, u_k), +]\lambda_{k+1}^T [f(x_k, u_k) - x_{k+1}]. \quad (9)$$

By defining the Hamiltonian function as

$$H_k = L(x_k, \tilde{y}_k, u_k) + \lambda_{k+1}^T f(x_k, u_k). \quad (10)$$

In this case, Eq. (6) can be represented as in (Kim, 2003):

$$J = \phi(x_N) + \left[\lambda_N^T x_N + \sum_{k=1}^{N-1}\left[H_k - \lambda_N^T x_{N_k}\right] + H_0. \quad (11)\right.$$

Meanwhile, we need to selected $\{u_k\}^{N-1}$ that reduces *J*, we take a look at the expression for as in (Kim, 2003):

$$J = \left[\frac{\partial \phi}{\partial x_N} - \lambda_{N_k}^T\right] dx_N + \frac{\partial H_0}{\partial x_0} dx_0 + \frac{\partial H_k}{\partial \tilde{y}_0} d\tilde{y}_0 + \frac{\partial H_k}{\partial u_0} du_0 +$$

$$+ \sum_{k=1}^{N-1}\left[\left\{\frac{\partial H_k}{\partial x_k} - \lambda_k^T\right\} dx_k + \frac{\partial H_k}{\partial \tilde{y}_k} d\tilde{y}_k + \frac{\partial H_k}{\partial u_k} du_k\right]$$

Picking

$$-\lambda_N^T = \frac{\partial \phi}{\partial x_N} - \tilde{y}_N^T P_0 C, \quad (12)$$

$$-\lambda_k^T = + \frac{\partial H_k}{\partial \tilde{y}_k}\frac{\partial \tilde{y}_k}{\partial x_k} = \tilde{x}_k^T S + \lambda_{k+1}^T \frac{\partial f_k}{\partial x_k} - \tilde{y}^T Q C \quad (13)$$

yields

$$\Sigma - \sum_{k=1}^{N-1} \frac{\partial H_k}{\partial x_k} du_k + \lambda_0^T dx_0 \quad (14)$$

and

$$- \frac{\partial H_k}{\partial x_k} = u_k^T R + \lambda_{k+1}^T \frac{\partial f_k}{\partial u_k}. \quad (15)$$

With a primary rate of the input arrangement $\{\ \}\ \{u_k\}_0^{N-1}$ gained using a nonlinear predictive controller and an assumed $\{x_0\}\{x_k\}_1^N$ are first calculated using Eq. (5). Then, for $k = N,\ldots,1$, λ_k are calculated recursively using Eqs. (12)-(13), and for $k = N,\ldots,1$, λ_k, $\frac{\partial H_k}{\partial u_k}$ are calculated using Eq. (15) and used for the gradient descent. By setting u_k at the opening of the optimization, the iteration counts decrease meaningfully (Kim, 2003).

Through an original amount of the input series $\{\ \}\ \{u_k^{(0)}\}_0^{N-1}$ acquired via a nonlinear predictive controller and a known $\{x_0\}\{x_k\}_1^N$ are initially calculated applying expression (5). However, for $k = N,\ldots,1$, λ_k are computed recursively using expressions (12) and (13), and for $k = N,\ldots,1$, λ_k, $\frac{\partial H_k}{\partial u_k}$ are calculated with expression (15) and employed for the gradient incline. Via setting u_k at the beginning of the optimization at every time step with the u_k of the previous time trial, the iteration counts decrease substantially.

To permit more complex missions for intelligent autonomous TRDs, we have developed a multipurpose nonlinear controller that permits perfect hovering and precise trajectory tracking as well as waypoint navigation and moving target tracking. It takes as inputs mention trajectories (guidance system outputs) and state estimates (navigation system outputs) and creates forces and torques that are needed to control the vehicle's motion (Kendoul, 2009, Zosimovych, 2024).

This is accomplished by obtaining a mathematical model for smart TRD dynamics and developing its structural elements to convert it into two cascaded subsystems coupled by a nonlinear interconnection expression. A partial passivation purpose has been used to create control laws for each subsystem, so developing in a hierarchical and nonlinear inner–outer-loop controller. The inner loop with fast dynamics operates attitude tracking and creates the necessary torques. The outer loop with gradual dynamics is used to produce the thrust and the orientation angles required to follow a commanded translational trajectory. The asymptotic stability of the entire connected system is confirmed by the theories of systems in a cascade. The resultant nonlinear controller is therefore simple to employ and easy to tune, and it results in suitable flight performance (Kendoul, 2009, Zosimovych, 2024).

Let $\{e_1, e_2, e_3\}$ represent unit vectors along the respective inertial axes and $\{x_b, y_b, z_b\}$ symbolize unit vectors along the respective body axes.

In the presented study, the dynamical model considered for the control design and that can represent various TRD configurations including the quadrator helicopter is given by

$$m\ddot{\xi} = -\mathrm{u}R(\eta)\,e_3 + \mathrm{mg}e_3,$$

$$(\ )\ \dot{M}(\eta)\,\ddot{\eta} + C(\eta, \dot{\eta})\dot{\eta} = (\eta)^T\tau. \qquad (16)$$

The controller enterprise for nonlinear systems focuses on robust link bids with practical meaning and theoretical trials. In this research, the control design for medium-size smart TRDs is

addressed in the next steps (Kendal, 2009):

1. Uncouple the translational and attitude dynamics by converting the nonlinear model (16) into two linear subsystems coupled by a nonlinear interconnection term.
2. Create two independent controllers for the translation and rotation subsystems.
3. Verify the asymptotic stability of the complete-linked closed-loop system using cascaded system models.

Since the attitude dynamics in Eq. (16) is a completely actuated mechanical structure for $\theta \neq k\pi/2$, then it is precise feedback linearizable. In detail, by applying the change of variables [16]:

$$( )\tau^{\sim} = J\psi(\eta)(\tilde{\tau} +)\Phi^{T} C(\eta,\dot{\eta})\,\dot{\eta}, \qquad (17)$$

and we obtain a 3D double integrator where $^{\sim}\tilde{\tau}$ is a new control input. Therefore, the dynamics of the TRD in Eq. (16) converts into the next

$$\begin{aligned}
\ddot{x} &= -\tfrac{1}{m}u\left(\cos\phi\sin\theta\cos\psi + \sin\phi\sin\psi\right), \ddot{\phi} = \tilde{\tau}_{\phi},\\
\ddot{y} &= -\tfrac{1}{m}u\left(\cos\phi\sin\theta\sin\psi - \sin\phi\cos\psi\right), \ddot{\theta} = \tilde{\tau}_{\theta},\\
\ddot{z} &= -\tfrac{1}{m}u\cos\theta\cos\phi + g, \ddot{\psi} = \tilde{\tau}_{\psi}
\end{aligned} \qquad (18)$$

Our idea here is to suggest a multipurpose controller that can accomplish autonomous stabilization of the drone but also precise trajectory tracking for as position as attitude. These skills are needed to achieve several practical applications.

5. Results and Discussion

To estimate the performance of our test TRD, we presented real-time flight tests with numerous mission settings. Now, we present some test results from six flight tests that reveal the autonomous abilities of a test TRD, including correct attitude tracking, automatic take-off and landing, long-distance flight, waypoint navigation, trajectory tracking, and vision-based flight (Kendal, 2009, Zosimovych, 2024). The objective of these flight tests is to show that the developed drone, equipped with the designed autopilot, can autonomously realize the search and rescue mission described earlier.

Vol. 11, No. 01; 2026

ISSN: 2456-3676

In the attitude trajectory tracking flight test, we managed the attitude flight control to study the efficiency and robustness of the inner loop nonlinear controller. For reliable estimation of the attitude controller execution, an outdoor test was executed in which reference trajectories were generated in the following manner:

1. During 0 and 30 s, pre-programmed sinusoidal paths were created with a 0.5-Hz frequency and a time-varying magnitude. The pitch angle magnitude increases from 0 to 45 deg and the roll angle magnitude is set to 0 deg (0–20 s), then to 30 deg (20–20 s), and finally to 0 deg (20 s).
2. Between 20 and 120 s, the reference trajectories are delivered by the operator via the RC transmitter (semiautonomous control), such that the induced forward velocities are relatively high-level (about 4 m/s).

The attitude control effects are displayed in Fig. 6, where you can see the TRD precisely tracking the reference commands. Resulting tracking was gained even at comparatively large and quickly varying angles. Moreover, the controller manages to link between the pitch and roll axes even when the angles are large enough.

The nonlinear predictive controller allowing by next Eq.:

$$\| u = m \|\mu(\chi\|\ddot{\xi}_d) - \|ge_3\| = m \| - K_\chi \chi \| + \ddot{\xi}_d - ge_3 \|,$$
$$(\ ) \sim \quad (\ \tau) = J\psi(\eta)(\tilde{\tau}) + (\Phi^T C(\eta,\dot{\eta}))\dot{\eta} = J\psi(\eta)(\ddot{-}K_e e + \ddot{\eta}_d) + \Phi^T C(\eta,\dot{\eta})\,\dot{\eta}. \qquad (19)$$

and we find that a 3D is applied in flight tests to realize automatic take-off, precise hovering, and precise intelligent auto loading (Kendal, 2009). The trial results, established in Fig. 8, show the correct tracking of the height reference command, yielding to the actual altitude control and automatic take-off and landing. The smart TRD also succeeded in a stable hovering flight and could stay within a 0.5-m-radius circle. The horizontal movement is also truly controlled in take-off and landing movements with fewer than 1-m error, which is a good performance for this scale drone flying subject to external instability such as wind.

The goals of this flight test were to do the following:
1. Show the ability of our smart TRD to fly autonomously until the area of activity, placed at about 1 km from the launching point.
2. Confirm the quality and range of wireless communication and the video transmission.
   The drone was thus tasked to reach an autonomous forward flight at a translational velocity of 4.0 m/s while transferring images to the GCS.

During flight tests, we obtained results which show that the velocity and attitude reference trajectories are well tracked. The position trajectories show that the TRD flew a relatively long distance autonomously, which is about 2.0 km $\sqrt{\quad}(\sqrt{x^2 + y^2})$. When the smart TRD reached the checks of the fly region, the safety pilot turned to manual flight and retrieved the drone. The

Vol. 11, No. 01; 2026

ISSN: 2456-3676

test also indicated that the range of Wi-Fi wireless communication was about 500 m; however, the condition of the video transmission was acceptable up to 1,000 m. In those tests, the safety technique associated with communication lost was disabled, thus allowing the test drone to continue the mission completing even when the communication link was lost.

Furthermore, now, we show the capability of the tested system to complete precise waypoint navigation and to execute hovering and automatic intelligent take-off and landing. In those flight tests, a set of four waypoints were selected by simply clicking the desired locations on the two-dimensional (2D) map. The TRD should then pass the transferred waypoints in each series. These flight tests reproduce a reconnaissance mission in which the drone is tasked to fly some object areas for the information set.

The automatic intelligent take-off and landing abilities were also proved in the flight tests with perfect altitude control even at the relatively high horizontal speeds of 6 m/s. It is remarkable, however, to note that altitude control is more precise at low forward speeds with about 0.5-m squared error. The thrust variation produced by different angles of attack at varying forward speeds and wind conditions produces a disturbance that forces the drone above reference height. During those fly tests, the controller takes some time to reject the instability because of the time gap in thrust.

The concert of the autopilot for intelligent trajectory tracking is a crucial assessment. The last goal of the drone is to achieve autonomous search, rescue, and observation tasks. Hence, the trajectory tracking ability is extremely useful since a spiral trajectory following allows the experimental smart TRD to explore some spot of activity. Moreover, exact trajectory tracking is essential for accurate movements in covered conditions to avoid obstacles.

In those flight tests, a spiral curve was implemented to demonstrate the tracking performance of the nonlinear controller. The reference trajectory was generated using a kinematic model of a modified Archimedean spiral to obtain a spiral with a constant separation distance (10 m) between successive turnings and a constant tangential speed (2.5 m/s).

A probable nonlinear control method to control the hover drive is the feedback loop linearization technique [6], in which the nonlinear components are void (or have their effects tremendously reduced) over the feedback loop of a sufficiently selected control law. An ideal control law would build the following system with proportional control. Counting the examined system:

$$\dot{\rightarrow}\left(\rightarrow\right)\underset{V}{\dot{\rightarrow}}=\left(F_1\left(\underset{X}{\rightarrow}\right)\right)+h_2\left(\underset{U}{\rightarrow}\right), \tag{20}$$

$$\dot{\rightarrow}\left(\rightarrow\right)\underset{\Omega}{\dot{\rightarrow}}=\left(f_3\left(\underset{X}{\rightarrow}\right)\right)+h_4\left(\underset{U}{\rightarrow}\right). \tag{21}$$

The first derivative of the conditions regarding time would be obtained by the resulting mathematical term:

$$\dot{\vec{X}} = f_3\left(\vec{X}\right) + \begin{bmatrix} \int \dot{\vec{V}} \\ \dot{\vec{V}} \\ \int \dot{\vec{\Omega}} \\ \dot{\vec{\Omega}} \end{bmatrix}. \tag{22}$$

Agree to $\dot{\vec{V}}, \dot{\vec{\Omega}}$ occur an ideal control law that would product in (Kendoul, 2009):

$$\dot{\vec{V}} = F_1\left(\vec{X}\right) + h_2\left(\vec{U}^*\right) - K\vec{X} + F_1\left(\vec{X}\right) \cong -K_1\left(\vec{X}\right) + w_v, \tag{23}$$

$$\dot{\vec{\Omega}} = f_3\left(\vec{X}\right) + h_4\left(\vec{U}^*\right) - K\vec{X} + f_3\left(\vec{X}\right) \cong -K_2\left(\vec{X}\right) + w_\Omega. \tag{24}$$

Here w_v and w_Ω are nonlinear noises and disturbances affecting the system. If possible, the noise and disturbances should be such that (Kendal, 2009):

$$\left| K\vec{X} \right| \gg w_v, \tag{25}$$

$$\left| K\vec{X} \right| \gg w_\Omega. \tag{26}$$

Thinking of the next two equations from (Kendal, 2009):

$$h_2\left(\vec{U}^*\right) = \frac{\vec{F}_{prop}\left(\vec{U}\right)}{m}, \tag{27}$$

$$h_4\left(\vec{U}^*\right) = J^{-1}\left[\vec{M}_{prop}\left(\vec{U}\right) + \vec{M}_{gyro}\left(\vec{U}\right)\right]. \tag{28}$$

After expending both equations above and presumed for the hover movement that the drone has both propellers in the vertical position, that is, with zero tilt. These assumptions reduce all previous equations to the following:

$$\begin{cases} \delta_{lp} = \delta_{rp} = 0 \\ \cos(0) \\ \sin(0) \end{cases}, \tag{29}$$

$$h_2\left(\vec{U}\right) = \frac{1}{m}\begin{bmatrix} 0 & 0 & 0 \\ 0 & 0 & 0 \\ -1 & -1 & -1 \end{bmatrix}\begin{bmatrix} sgn(\omega_{lp})k_{lp}\omega_{lp}^2 \\ sgn(\omega_{rp})k_{rp}\omega_{rp}^2 \\ sgn(\omega_{bp})k_{bp}\omega_{bp}^2 \end{bmatrix}, \tag{30}$$

$$h_4\left(\vec{U}\right) = J^{-1}\left[\begin{bmatrix} J_{xx} & J_{xx} & 0 \\ J_{yx} & J_{yx} & 0 \\ J_{zx} & J_{zx} & 0 \end{bmatrix}\begin{bmatrix} sgn\left(\omega_{lp}\right)k_{lp}\omega_{lp}^2 \\ sgn\left(\omega_{rp}\right)k_{rp}\omega_{rp}^2 \\ sgn\left(\omega_{bp}\right)k_{bp}\omega_{bp}^2 \end{bmatrix}\right] +$$

$$J^{-1}\left[\begin{bmatrix} -y_{cm\to lp} & -y_{cm\to rp} & -y_{cm\to bp} \\ x_{cm\to lp} & x_{cm\to rp} & x_{cm\to bp} \\ 0 & 0 & 0 \end{bmatrix}\right]\begin{bmatrix} sgn\left(\omega_{lp}\right)k_{lp}\omega_{lp}^2 \\ sgn\left(\omega_{rp}\right)k_{rp}\omega_{rp}^2 \\ sgn\left(\omega_{bp}\right)k_{bp}\omega_{bp}^2 \end{bmatrix}. \qquad (31)$$

Deciding as a primary model for the control law:

$$\rightarrow \quad \begin{bmatrix} \sqrt{} \\ \sqrt{} \\ \sqrt{} \\ \end{bmatrix} \underset{U}{\rightarrow} = \begin{bmatrix} \sqrt{\omega_{lp}} \\ \sqrt{\omega_{rp}} \\ \sqrt{\omega_{bp}} \\ 0 \\ 0 \end{bmatrix} - K\underset{X}{\rightarrow}, \qquad (32)$$

$$\left(\rightarrow\right) \quad -\left[\qquad\qquad\right]\left[\qquad\qquad h_2\left(\underset{U}{\rightarrow}\right) = \frac{1}{m}\begin{bmatrix} 0 & 0 & 0 \\ 0 & 0 & 0 \\ -1 & -1 & -1 \end{bmatrix}\begin{bmatrix} sgn(\omega_{lp})k_{lp}\omega_{lp} \\ sgn(\omega_{rp})k_{rp}\omega_{rp} \\ sgn(\omega_{bp})k_{bp}\omega_{bp} \end{bmatrix},$$

(33)

$$h_4\left(\underset{U}{\rightarrow}\right) = J^{-1}\left[\begin{bmatrix} J_{xx} & J_{xx} & 0 \\ J_{yx} & J_{yx} & 0 \\ J_{zx} & J_{zx} & 0 \end{bmatrix}\begin{bmatrix} sgn(\omega_{lp})k_{lp}\omega_{lp} \\ sgn(\omega_{rp})k_{rp}\omega_{rp} \\ sgn(\omega_{bp})k_{bp}\omega_{bp} \end{bmatrix}\right] +$$

$$\left[\left[\qquad\qquad\right]\right]\begin{bmatrix} \\ \\ \end{bmatrix}$$

$$J^{-1}\left[\begin{bmatrix} -y_{cm\to lp} & -y_{cm\to rp} & y_{cm\to bp} \\ x_{cm\to lp} & x_{cm\to rp} & -x_{cm\to bp} \\ 0 & 0 & 0 \end{bmatrix}\right]\begin{bmatrix} sgn(\omega_{lp})k_{lp}\omega_{lp} \\ sgn(\omega_{rp})k_{rp}\omega_{rp} \\ sgn(\omega_{bp})k_{bp}\omega_{bp} \end{bmatrix}. \qquad (34)$$

This proposition for a potential control law is not passed to stabilize the system because MATLAB's function 'place' and 'dlqr' here unable to find correct gain matrices K. This indicates that a more robust and complicated control procedure is essential. A different opportunity to study is the further use of linearization, incorporating the linearization of the input. By employing the Taylor series to the description of the rotor force, it is feasible to convert it into a piecewise equation, such that, created a specific boundary, it is linear inside that boundary (Kendal, 2009):

Vol. 11, No. 01; 2026

ISSN: 2456-3676

$$\left\{ \begin{array}{l} \longrightarrow \Big|_{\rightarrow} \longrightarrow \longrightarrow \left\{ \begin{array}{l} F_{\text{rot}}(\underset{\omega_{\text{rot}}}{\longrightarrow})\Big|_{\underset{\omega^*}{\rightarrow}} \cong \alpha + \beta(\underset{\omega_{\text{rot}}}{\longrightarrow} - \overrightarrow{\omega^*}) \\ \alpha = k_{\text{rot}}\overrightarrow{\omega^*}^2 \\ \beta = 2k_{\text{rot}}\overrightarrow{\omega^*} \end{array} \right. \\ \longrightarrow \\ \longrightarrow \end{array} \right. . \quad (35)$$

The alternative does not resolve; however, the nonlinearities raise the tilting of the rotors and the combination of the states. An unconventional potential key is to realize a rolling-mode output-feedback linearization as offered on (Bartolini, 2012). However, that publication does not cover some essential parts such as strategies to specify a sufficient tilting manifold.

6. Conclusion and Future Work

Even though there have been upright samples of autonomous control of tilt-rotor drones and obtained results represent substantial innovations for autonomous intelligent drones:

1. From a control system viewpoint, we have designed a hierarchical model-based nonlinear controller that has the following benefits:

- it believes in system nonlinearities and links while guaranteeing the asymptotic stability of the closed loop system;
- it is a versatile controller that can supervise various flight modes such as hovering, flying forward, flying sideward, take-off and landing, and trajectory tracking;
- it is simple to apply and easy to tune online even when the plant factors are not well identified.

4. We have carefully chosen lightweight avionics components that fit the partial payload of miniature intelligent drones, and we have designed an embedded real-time architecture that contains navigation sensors, GPS, pressure sensor (PS), mission sensors (camera), a flight control computer (FCC), and a WI-FI communication module. In contrast to other tests reported in the literature, we do not trust any precise IMU or GPS whose costs and weights are considerably higher. We believe that the cost decrease will yield a significant speedup of the use of drones for civilian applications.
5. From a drone system integration perspective, we have settled and employed guidance, navigation, and vision algorithms that present advanced autonomous behaviors to tilt-rotor drones (TRD) that weigh up to 200 kg.
6. From an experimental perspective, we performed several flight tests in outdoor and natural environments using a smart TRD. The drone, equipped with the developed autopilot, has undergone an extensive program of flight tests, resulting in various autonomous flight behaviors (automatic take-off and landing, accurate hovering, long-distance flight, waypoint navigation, trajectory tracking, and vision-based target tracking).
7. The next recommended stage would be the application of robust control laws and methods such as adaptive control, feedback stabilization, sliding mode control, and extremum seeking control by the detached of the supervisory system without additional simplifications and specific expectations.

Vol. 11, No. 01; 2026

ISSN: 2456-3676

It is evident that the proposed model needs advanced control methods, numerous of which are new to the field of control and intelligent automation. The absence of acceptable mathematical models for this UAS concept validates the perception that this type of drone is at rest an object to to control, expecting advances and findings of new AI control systems.

References

CH-10 Rainbow-10 tilt-rotor VTOL shipboard reconnaissance strike drone, GlobalSecurity.org. (n.d.). Retrieved from https://www.globalsecurity.org/military/world/china/ch-10.htm

Sheng, Y., Xuanzun, L., China reveals the CH-10 tilt-rotor drone. Global Times, 2018. Retrieved from https://www.globaltimes.cn/page/201810/1125359.shtml

Vertical-landing Bayraktar, January 12, 2023. Retrieved from https://baykartech.com/en/press/vertical-landing-bayraktar-diha-drone-completes-flight-test-at-8000-ft/

Çakıcı, F., Leblebicioglu, K., Modeling and simulation of a small-sized tiltrotor UAV, The Journal of Defense Modeling & Simulation, 9(4), 335-345, 2012. Retrieved from https://www.researchgate.net/publication/258132199_Modeling_and_simulation_of_a_small-sized_Tiltrotor_UAV

Wang, H., Sun, W., Zhao, C., Zhang, J., Dynamic modeling and control for tilt-rotor UAV based on 3D flow field transient CFD, MDPI. Retrieved from https://www.mdpi.com

Pessoa, R. S. Mathematical modeling of a tilt-rotor drone. Projeto de Graduação, Pontifícia Universidade Católica do Rio de Janeiro, Brazil, 2017. Retrieved from https://www.maxwell.vrac.puc-rio.br/30497/30497.PDF

"Design, modeling and control for a tilt-rotor VTOL UAV in the presence of actuator failure", in Proceedings of the IEEE/RSJ Int. Conf. on Intelligent Robots and Systems (IROS), pp. 4310-4317. Retrieved from https://arxiv.org/abs/2205.05533

Duncombe, J. U. "Infrared navigation—Part I: An assessment of feasibility," IEEE Transactions Electron Devices, vol. ED-11, no. 1, pp. 34–39, 1959. W. L. Brogan, Modern control theory (3rd ed.). Retrieved from https://dokumen.tips/documents/william-l-brogan-modern-control-theory-3rd-edibookfiorg.html?page=1

Stevens, B. L., Lewis, F. L., Johnson, E. N. (2016), Aircraft control and simulation: Dynamics, control design, and autonomous systems, 3rd ed.: Wiley.

"Federal Aviation Administration (FAA)" in Advanced avionics handbook: Department of Transportation, U.S., 2009.

Kay ton, M., Friend, W. R. (2006), "Avionics navigation systems" in Wiley-Interscience, 2nd ed.

Vidmar, R. J. "On the use of atmospheric plasmas as electromagnetic reflectors," IEEE Transactions on Plasma Sciences, vol. 21, issue 3, pp. 876–880, 1992.

Kim, H. J., Shim, D. H. A flight control system for aerial robots: Algorithms and experiments. Control Engineering Practice, 11(12), pp. 1389-1400, 2003. Retrieved from https://people.eecs.berkeley.edu/~sastry/pubs/PDFs%20of%20Pubs2000-2005/Pdfs%20of%20Misc.%20Others/Kim,H.Jin/KimFlightControlSystem2003.pdf

Vol. 11, No. 01; 2026

ISSN: 2456-3676

Zosimovych, N. "UAV autopilot controller with test dynamics model platform", in XI Int. Sc. and Eng. Conf. (IKT-2020), Zhytomyrska Polytechnic Publisher, Zhytomyr, Ukraine, pp. 135-138, 2020.

Emobility Engineering, (n.d.), Virtual AC system controllers. Retrieved from https://www.emobility-engineering.com/virtual-ac-system-controllers/

Zosimovych, N. "UAV autopilot controller with test dynamics model platform", in XI Int. Sc. and Eng. Conf. (IKT-2020), Zhytomyrska Polytechnic Publisher, Zhytomyr, Ukraine, pp. 135-138, 2020. N. Zosimovych, "Tilt-rotor drone-flight control system design", in XXII Int. Sc. and Pract. Conf. Proc.: Modern Theories and Improvement of World Methods, Helsinki, Finland, pp. 433-440, June 6–9, 2023. Retrieved from https://isg-konf.com/uk/modern-theories-and-improvement-of-world-methods/

Kendoul, F., Zhenyu, Y., Nomanami, K. Guidance and nonlinear control system for autonomous flight of mini rotorcraft unmanned aerial vehicles, Journal of Field Robotics, 2009.

Zosimovych, N. "A flight control system for tilt-rotor drone", in Webinar V-MAE2024, 3rd Edition of Mechanical and Aerospace Eng. Virtual Program, 2024. Retrieved from https://www.sciwideonline.com/v-mae2024/#scientifictopics

Zosimovych, N. Hierarchical flight control system for tilt-rotor drones. Transactions on Eng. and Computing Sc., 12(3), pp. 73-87, 2024. Retrieved from https://journals.scholarpublishing.org/index.php/TMLAI/article/view/17047

Zosimovych, N. Hierarchical flight control system for tilt-rotor drones. Journ. of Eng. and Appl. Sc. Technol., 6(5), pp. 1-7, 2024). Retrieved from https://onlinescientificresearch.com/articles/hierarchical-flight-control-system-for-tiltrotor-drones.pdf

Bartolini, G., Punta, E. Sliding mode output-feedback stabilization of uncertain nonlinear non-affine systems. Automatic, 48(12), pp. 3106-3113, 2012. Retrieved from https://www.researchgate.net/publication/256660653_Sliding_mode_output-feedback_stabilization_of_uncertain_nonlinear_nonaffine_systems